Hindawi
International Journal of Photoenergy
Volume 2021, Article ID 8842975, 12 pages
https://doi.org/10.1155/2021/8842975

Research Article

Performance Optimization of the InGaP/GaAs Dual-Junction Solar Cell Using SILVACO TCAD

Marwa S. Salem,[1,2] **Omar M. Saif**,[3] **Ahmed Shaker**,[4] **Mohamed Abouelatta**,[5] **Abdullah J. Alzahrani**,[1] **Adwan Alanazi**,[1] **M. K. Elsaid**,[5] **and Rabie A. Ramadan**[1,6]

[1]*Department of Computer Engineering, College of Computer Science and Engineering, University of Ha'il, Ha'il, Saudi Arabia*
[2]*Department of Electrical Communication and Electronics Systems Engineering, Faculty of Engineering, Modern Science and Arts University (MSA), Cairo, Egypt*
[3]*Canadian International College, Engineering School, Giza, Egypt*
[4]*Engineering Physics and Mathematics Department, Faculty of Engineering, Ain Shams University, Cairo, Egypt*
[5]*Department of Electronics and Communications, Faculty of Engineering, Ain Shams University, Cairo, Egypt*
[6]*Department of Computer Engineering, Faculty of Engineering, Cairo University, Cairo, Egypt*

Correspondence should be addressed to Rabie A. Ramadan; rabie@rabieramadan.org

Received 6 July 2020; Revised 31 December 2020; Accepted 8 February 2021; Published 19 February 2021

Academic Editor: Elias Stathatos

In this work, an optimization of the InGaP/GaAs dual-junction (DJ) solar cell performance is presented. Firstly, a design for the DJ solar cell based on the GaAs tunnel diode is provided. Secondly, the used device simulator is calibrated with recent experimental results of an InGaP/GaAs DJ solar cell. After that, the optimization of the DJ solar cell performance is carried out for two different materials of the top window layer, AlGaAs and AlGaInP. For AlGaAs, the optimization is carried out for the following: aluminum (Al) mole fraction, top window thickness, top base thickness, and bottom BSF doping and thickness. The electrical performance parameters of the optimized cell are extracted: $J_{SC} = 18.23\,\text{mA/cm}^2$, $V_{OC} = 2.33\,\text{V}$, FF = 86.42%, and the conversion efficiency (η_c) equals 36.71%. By using AlGaInP as a top cell window, the electrical performance parameters for the optimized cell are $J_{SC} = 19.84\,\text{mA/cm}^2$, $V_{OC} = 2.32\,\text{V}$, FF = 83.9%, and $\eta_c = 38.53\%$. So, AlGaInP is found to be the optimum material for the InGaP/GaAs DJ cell top window layer as it gives 4% higher conversion efficiency under 1 sun of the standard AM1.5G solar spectrum at 300 K in comparison with recent literature results. All optimization steps and simulation results are carried out using the SLVACO TCAD tool.

1. Introduction

There has been a trend for shifting energy production by renewable energy resources especially solar energy which is considered the most favorable resource as it is safe and clean [1, 2]. There are many emerging technologies to capture the energy from the sun [3, 4]. Photovoltaic technology is the most widely used technology [5–8]. Among photovoltaic technologies, the multijunction solar cell gives higher efficiency in comparison with the silicon-based solar cells [9]. The multijunction solar cells' idea depends on stacking p-n junctions with different bandgaps which permits the absorbance of a wider range of wavelengths [10, 11]. Among the multijunction solar cells, the III-V semiconductor compound-based solar cells are the commercially available cells with the highest reported efficiency [12, 13] reaching 46% under high solar concentration [2, 3]. In this regard, the InGaP alloy is a vital material for high-efficiency solar cells as it absorbs the visible part of the solar spectrum [14–16]. Besides, the GaAs compound (1.42 eV) absorbs the Near-Infrared Region (NIR) of the spectrum. Therefore, the lattice-matched $In_{0.49}Ga_{0.51}P$ grown on the GaAs substrate has great technological importance as the InGaP/GaAs solar cell structure absorbs a substantial part of the spectrum [15, 17]. So, InGaP/GaAs DJ solar cells have been widely studied due to their superb bandgap arrangement in lattice-matched systems [18].

In 2006, Lueck et al. designed a dual-junction InGaP/GaAs solar cell exhibiting an efficiency of about 23.6% at 1 sun concentration [19]. A few years later, Leem et al. modeled and simulated InGaP/GaAs dual-junction solar cells using the InGaP/InGaP tunnel junction having an efficiency of 25.28% at AM1.5G [20]. In 2011, Singh and Sarkar developed an effective approach for highly efficient solar cells using virtual wafer fabrication (VWF) tools. The maximum conversion efficiency achieved from such an approach is 32.20% and 36.67% at 1 sun and 1000 suns, respectively. Such efficiencies were obtained under AM1.5G illumination [21]. Singh and Sarkar, in 2012, devised an ARC-less InGaP/GaAs cell having an optimized $In_{0.5}(Al_{0.7}Ga_{0.3})_{0.5}P$ bottom BSF layer. Regarding this structure, the cell parameters $J_{SC} = 16.09\,mA/cm^2$, $V_{OC} = 2.66\,V$, and FF = 89.50% were found under AM1.5G illumination and the maximum efficiency was 32.196% and 36.678% for 1 sun and 1000 suns, respectively [22]. In 2015, a GaInP/-GaAs DJ cell was simulated employing the SILVACO TCAD device simulator tool by Nayak et al. The simulation gave $J_{SC} = 17.33\,mA/cm^2$, $V_{OC} = 2.66\,V$, and FF = 88.67% revealing a maximum efficiency of 34.52% and 39.15% at 1 sun and 1000 suns, respectively [23].

In recent research studies, a double-layer back surface field (BSF) is included in both the top and bottom layers of the DJ solar cell. Thus, the performance of the InGaP/GaAs cell is enhanced due to the improvement in the collection of photogenerated minority carriers. In addition, the efficiency of such a cell was optimized to 40.879% (1000 suns) by varying the thicknesses of the top BSF layer [24]. In addition, Chee and Hu modeled and numerically simulated an InGaP/GaAs DJ cell [25]. The mentioned study focused on varying some design parameters like tunnel junction materials and back surface field layer composition and thickness yielding J_{SC} of $20.71\,mA/cm^2$, V_{OC} of 2.44 V, and FF of 88.6% and guaranteeing a maximum efficiency of 32.4% under 1 sun AM0 illumination. Also, Djaafar and Hadri studied the variation of thickness and doping concentration of the emitter and the base in addition to the molar fraction of the emitter to optimize the performance of InGaP/GaAs. The optimization at 300 K led to J_{SC} of $15.19\,mA/cm^2$, V_{OC} of 2.53 V, FF of 91.32%, and an efficiency of 25.43% [26]. In 2019, Hungyo et al. optimized the InGaP/GaAs DJ solar cell by varying the emitter and base thicknesses alongside temperature variation [27]. Furthermore, Oshima et al. inspected experimentally the growth of InGaP on the GaAs substrate by Solid-Source Molecular Beam Epitaxy (SS-MBE). They found an increase in the open-circuit voltage of InGaP from 1.243 V to 1.311 V. Using such a design, the highest 25.57% efficiency could be obtained for the InGaP/-GaAs DJ solar cell [15]. Moreover, InGaP/GaAs DJ solar cells have been fabricated using hydride vapor phase epitaxy (HVPE) [28]. The open-circuit voltage was measured as 1.339 V and 0.978 V for individually InGaP and GaAs subcells, respectively. Hence, the total V_{OC} is 2.318 V yielding 21.89% conversion efficiency.

As mentioned above, many research works have been conducted to increase the efficiency of the InGaP/GaAs DJ cells; however, more efforts are still required to get higher efficiencies. The complexity of the DJ cell structures, due to their many layers parameters, makes it difficult to optimize the performance experimentally. So, numerical TCAD simulations are very helpful to optimize the cell performance and to understand the major physical behaviors, thus decreasing the development time and cost. An effective window layer is a crucial structural element for a high-efficiency multijunction cell. The main contribution of this work is to optimize the InGaP/GaAs DJ solar cell performance for two different top window layers, AlGaAs and AlGaInP. We give a comprehensive comparison between the two materials to show the criteria for choosing the best top window layer material. Thus, the optimum top window layer, which gives the maximum efficiency, is determined.

The remainder of the paper is arranged as follows. Firstly, in Section 2, the design of our InGaP/GaAs DJ solar cell is illustrated. Besides, the simulation models and calibration vs. measurements are provided. Then, in Section 3, the optimization of the InGaP/GaAs DJ solar cell performance is accomplished numerically considering the two different materials of the top window layer: AlGaAs and AlGaInP. For each window layer case, the optimization technique is organized as follows: the composition of the top window material is optimized. Using the optimized value of the composition, the top window layer thickness is optimized and then the top base thickness is tuned. Furthermore, the bottom BSF optimum doping and thickness are investigated to obtain the maximum allowable conversion efficiency. Next, the I-V characteristic, P-V curve, and external quantum efficiency (EQE) of the two optimized InGaP/GaAs DJ solar cells are provided. In addition, the electrostatic potential and photogeneration rates are presented. Finally, a comparison between the performances of the two optimized InGaP/GaAs DJ solar structures is utilized and the optimum material for the top window layer is selected. Moreover, in Section 4, the performance of the optimum InGaP/GaAs DJ solar cell structure is compared with the recent previous studies. Finally, a summary of the essential findings and conclusions of this work is drawn in Section 5. All simulations are performed using SILVACO TCAD.

2. Design of the InGaP/GaAs DJ Solar Cell

In this section, firstly, the design of the InGaP/GaAs DJ solar cell structure is presented. Secondly, the required physical models for the solar cell design are explained. Finally, the selected materials with their required parameters used for the solar cell design are illustrated.

2.1. The InGaP/GaAs DJ Solar Cell Structure. Figure 1 shows the basic structure of the InGaP/GaAs DJ solar cell. Figure 1(a) shows the different layers of the structure while Figure 1(b) illustrates the cell structure using the SILVACO TCAD tool. As shown in Figure 1(a), the structure consists of the InGaP top cell and GaAs bottom cell. Both the top and bottom cells consist of five layers: window, p-type emitter, n-type base, and two BSF layers. To enhance the performance of the structure, the top and bottom cells are connected through a GaAs/GaAs tunnel diode which must be transparent. It has not absorbed any part of the input solar radiation

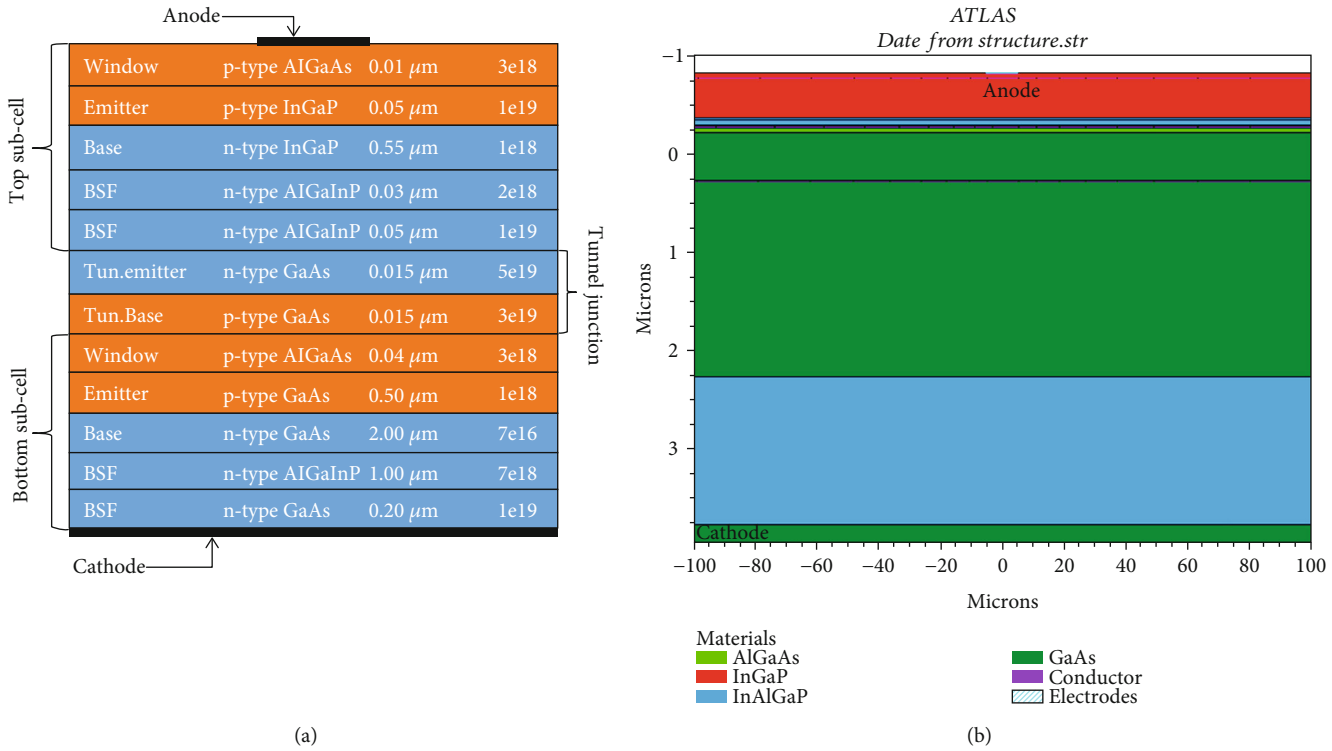

FIGURE 1: Schematic diagram of the InGaP/GaAs DJ solar cell structure. (a) Different layers showing the used materials with their thicknesses and doping levels. (b) Presented solar cell structure output from the SILVACO TCAD tool.

spectrum from the bottom side. Such requirements are achieved by satisfying two designing conditions. The first condition is that the diode has to be heavily doped. The second condition is that both the n-side and the p-side of the diode have to be very thin, in the nanometer range [29].

2.2. Physical Models for the Design of the InGaP/GaAs DJ Solar Cell. The simulation of the DJ solar cell is performed by using the SILVACO ATLAS tool. In order to optimize the solar cell effectively, the physical models incorporated in the simulation should be selected carefully. The main physical models used for the design of any solar cell are concentration-dependent low field mobility, optical recombination, Shockley-Read-Hall, Auger recombination, and Fermi statistics. Regarding the DJ cell, the nonlocal band-to-band tunneling should be enabled in order to model the tunneling through the tunnel junction between the top and bottom cells. Table 1 summarizes the physical models used for designing the DJ solar cell in the SILVACO ATLAS simulator [30].

2.3. The Selected Materials for the Design of the InGaP/GaAs DJ Solar Cell. To design an optimized DJ solar cell, the materials used for each of its five layers should be selected and their parameters have to be determined. For both the top and bottom window materials, its lattice constant should be matched with the emitter material. In addition, it must have a wide energy gap compared with the emitter material [31]. There are different materials used for the design of the top window layer such as $Al_{(x)}Ga_{(1-x)}As$ and $(Al_{(x)}Ga_{(1-x)})_{(1-y)}In_yP$. These materials satisfy the design requirements.

For the top and bottom cells, the emitter and base materials are InGaP and GaAs, respectively. These materials are selected such that the energy gap of the top cell is higher than that of the bottom cell. Therefore, the top cell absorbs the short wavelengths and the bottom cell absorbs the long wavelengths of the input solar radiation spectrum [23, 32]. The material of the two BSF layers is selected to passivate the surface recombination among the base of the top cell and the emitter of the GaAs tunnel diode. Also, it has to passivate the tunnel diode contact and the substrate of the bottom cell [23, 24]. The materials of the two BSF layers must be lattice-matched with the GaAs of both the top and bottom cells having a higher energy gap compared with the base of the bottom cell. Both $(Al_{0.7}Ga_{0.3})_{0.5}In_{0.5}P$ and GaAs satisfy the design requirements of the BSF. Table 2 summarizes the main required parameters of the optimum selected materials which are used for the design of the InGaP/GaAs DJ solar cell. The materials' parameters shown in the table are the used parameters for the simulation of the DJ solar cell using the SILVACO ATLAS device simulator.

2.4. SILVACO ATLAS TCAD Tool Calibration. Before starting the optimization procedure for the InGaP/GaAs cell performance, the used device simulator, SILVACO ATLAS TCAD tool, is calibrated with recent experimental results of an InGaP/GaAs cell [36]. The tool is calibrated by using the same parameters of the reference solar cell. Thus, the tool calibration includes the same materials, thicknesses, and

Table 1: Basic physical models used in SILVACO ATLAS simulation.

Model	Syntax	Description
Mobility	CVT	To enable transverse field, doping, and temperature-dependent parts of mobility
Optical recombination	OPTR	To enable band-to-band recombination for direct band semiconductors
Shockley-Read-Hall	SRH	To enable recombination. It uses fixed minority carrier lifetimes
AUGER recombination	AUGER	To enable direct transition of three carriers. Important at high current densities
Fermi distribution	Fermi	To enable carrier statistics. Suitable for highly doped regions
Nonlocal band-to-band tunneling	BBT.NONLOCAL	To enable the spatial tunneling occurring through the top and bottom cells

Table 2: Main required parameters of the optimum selected materials used for designing the InGaP/GaAs DJ solar cell [33–35].

	$In_{0.49}Ga_{0.51}P$	GaAs	$Al_{0.8}Ga_{0.2}As$	$(Al_{0.7}Ga_{0.3})_{0.5}In_{0.5}P$
Lattice constant (Å)	5.65	5.65	5.65	5.65
Energy band gap (eV)	1.9	1.42	2.09	2.4
Permittivity	11.62	13.2	11.7	11.7
Affinity (eV)	4.16	4.07	3.53	4.2
MUN (cm^2/Vs)	1945	8800	212.2	2150
MUP (cm^2/Vs)	141	400	67.6	141
NC300 (/cm^3)	1.3*e*20	4.35*e*17	1.58*e*19	1.2*e*20
NV300 (/cm^3)	1.28*e*19	1.29*e*19	1.5*e*19	1.28*e*19
TAUN (s)	1*e* − 9	1*e* − 9	1*e* − 9	1*e* − 9
TAUP (s)	1*e* − 9	2*e* − 8	2*e* − 8	1*e* − 9

Table 3: TCAD simulation results for the calibrated cell in comparison with measurements.

	V_{OC} (V)	J_{SC} (mA/cm^2)	FF (%)	η (%)
Reference solar cell results [33]	2.392	16.1	87.52	32.196
TCAD calibration results	2.29	16.12	87.42	32.17

doping concentrations for all layers. Also, the calibration procedure utilizes the same physical models for the reference InGaP/GaAs cell. Table 3 shows that the simulation results for the calibrated solar cell are close to the measurements presented in the reference solar cell [36].

3. Performance Optimization of the InGaP/GaAs DJ Solar Cell Using Two Different Top Window Layers

The top widow layer of the InGaP/GaAs DJ solar cell effectively affects its overall performance significantly. There are different materials used as the top window layer. Both $Al_{(x)}Ga_{(1-x)}As$ and $(Al_{(x)}Ga_{(1-x)})_{(1-y)}In_yP$ used as these materials satisfy the design requirements and allow the performance enhancement of the InGaP/GaAs cell [31, 37, 38].

In this section, the InGaP/GaAs DJ solar cell performance is optimized regarding the two different materials of the top window layer: AlGaAs and AlGaInP. For each top window layer, the optimization of its parameters required for enhancing the DJ solar cell performance is illustrated. A comparison between using AlGaAs and using AlGaInP as the DJ solar cell top window layer is presented. Thus, the layer which achieves better performance and gives higher efficiency is selected as the optimum top window layer for the DJ solar cell.

3.1. Using AlGaAs as the Top Window Layer. In this section, simulations are carried out by utilizing AlGaAs as the material for the top window layer. Firstly, the optimization of the mole fraction for Al is investigated. Secondly, the optimization of the top window layer thickness is inspected. Then, the top base layer thickness is adjusted. After that, the optimization of the bottom BSF layer doping and thickness is performed. Then, the optimum performance of the DJ solar cell using AlGaAs is compared with the results of the optimized structure used for calibration. Finally, the *I-V* characteristic, *P-V* curve, external quantum efficiency (EQE), and generation rates of the optimized cell are reported.

3.1.1. Al Mole Fraction Optimization. It is important to select the best mole fraction (x) value for the compound semiconductor to satisfy the lattice matching between the different alloys [39, 40]. The refractive index (n) and the extinction coefficient (k) of the compound semiconductor vary based on its mole fraction [41]. Thus, to achieve the best values of such parameters which enhance the solar cell performance,

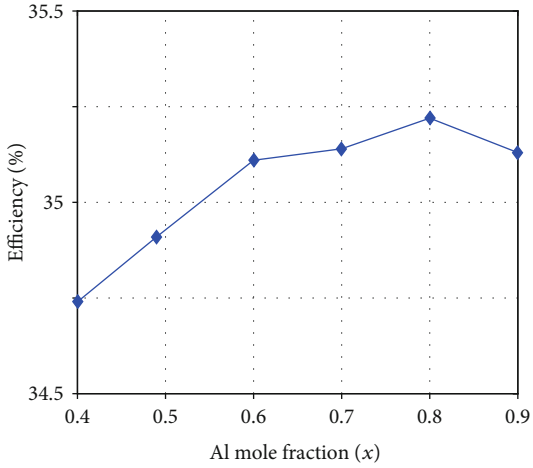

Figure 2: DJ solar cell efficiency for the six values of the Al mole fraction.

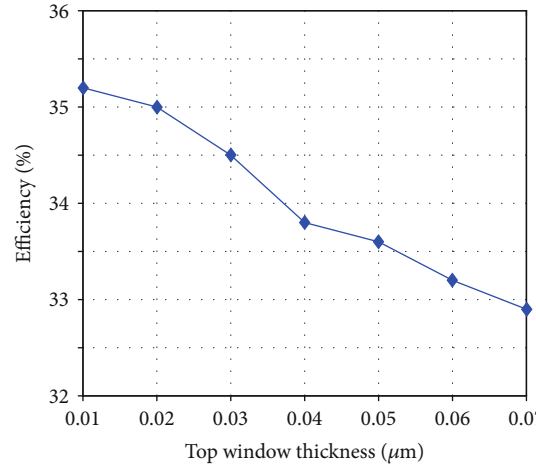

Figure 3: Cell efficiency vs. top window layer thickness.

the mole fraction of the compound semiconductor has to be optimized. Six values of the AlGaAs mole fraction are studied, and the efficiency of the InGaP/GaAs DJ cell is extracted for each value as shown in Figure 2. It can be inferred from the figure that the maximum efficiency of 35.22% occurs at x equals 0.8. Thus, the optimum compound of the AlGaAs which gives the maximum efficiency of the DJ solar cell is $Al_{0.8}Ga_{0.2}As$.

3.1.2. Optimization of the Top Window Layer Thickness. There are two main objectives of using the top window layer in the DJ solar cell. Firstly, it is used to reduce the surface recombination of the solar cell [7, 42]. Secondly, it must be transparent to enable the absorption of the whole input solar radiation spectrum [7, 31]. The first objective is achieved by optimizing the doping concentration of the top window layer. The optimum doping concentration for such a layer is 3×10^{18} cm^{-3} [20–24]. The second objective is satisfied by optimizing the layer thickness. Figure 3 shows the efficiency of the presented cell at different studied values of the top window layer thickness. The optimum thickness is 0.01 μm which gives 35.22% efficiency.

3.1.3. The Optimization of the Top Base Layer Thickness. Generally, in the solar cell design, the optimum base thickness should be less than the carrier diffusion length. So, the light-generated carriers are separated and collected by the solar cell p-n junction before recombination [6, 42]. The same concept is applied for the InGaP/GaAs DJ solar cell. The top base in the solar cell structure is n-type with 10^{18} cm^{-3} doping. Figure 4 presents the efficiency of the DJ solar cell vs. the variation in the top base thickness. Based on this simulation, the thickness of 0.4 μm is chosen as an optimum thickness as it gives 35.9% efficiency.

3.1.4. Optimization of the Bottom BSF Layer Doping and Thickness. The main objective of the bottom BSF layer is the passivation of the solar cell back surface to reduce its surface recombination [43]. There are two main requirements for achieving such an objective. Firstly, the thickness

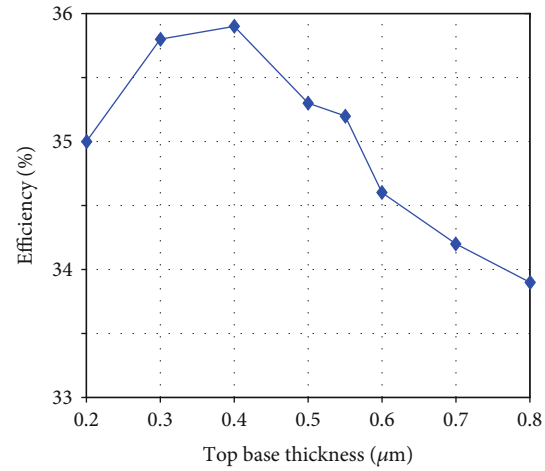

Figure 4: Cell efficiency vs. top base thickness.

of the BSF layer has to be relatively high to enhance the light absorption. Theoretically, there is a certain thickness of the BSF layer at which all the light will be absorbed. At such thickness, the DJ solar cell efficiency can reach its maximum. Beyond this thickness, there is a negligible change in the solar cell efficiency [35]. Figure 5(a) shows the efficiency of the DJ solar cell for different values of the bottom BSF layer thickness. As can be depicted, the efficiency increases when the layer thickness varies from 0.3 μm to 1 μm. Then, the efficiency is nearly fixed to its optimum value, 36.6%. Thus, the optimum bottom BSF layer thickness is 1 μm.

Further, the doping of the bottom BSF layer should be high [44]. Figure 5(b) illustrates the efficiency of the DJ solar cell variation w.r.t the bottom BSF layer doping concentration. The optimum doping concentration is 3×10^{19} cm^{-3}, which is the highest doping that gives an efficiency of 36.7%.

3.1.5. Electrical and Optical Performance. The simulated J-V characteristic and P-V curve using $Al_{0.8}Ga_{0.2}As$ as the top window material are presented in Figure 6(a). The extracted electrical performance parameters of this optimized DJ solar

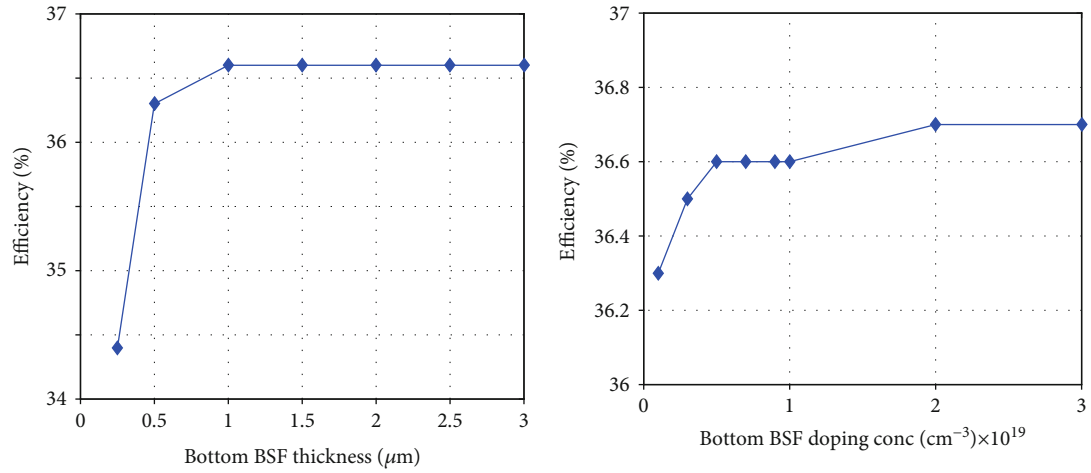

Figure 5: Optimization of the bottom BSF parameters. (a) Cell efficiency vs. thickness. (b) Cell efficiency vs. doping concentration.

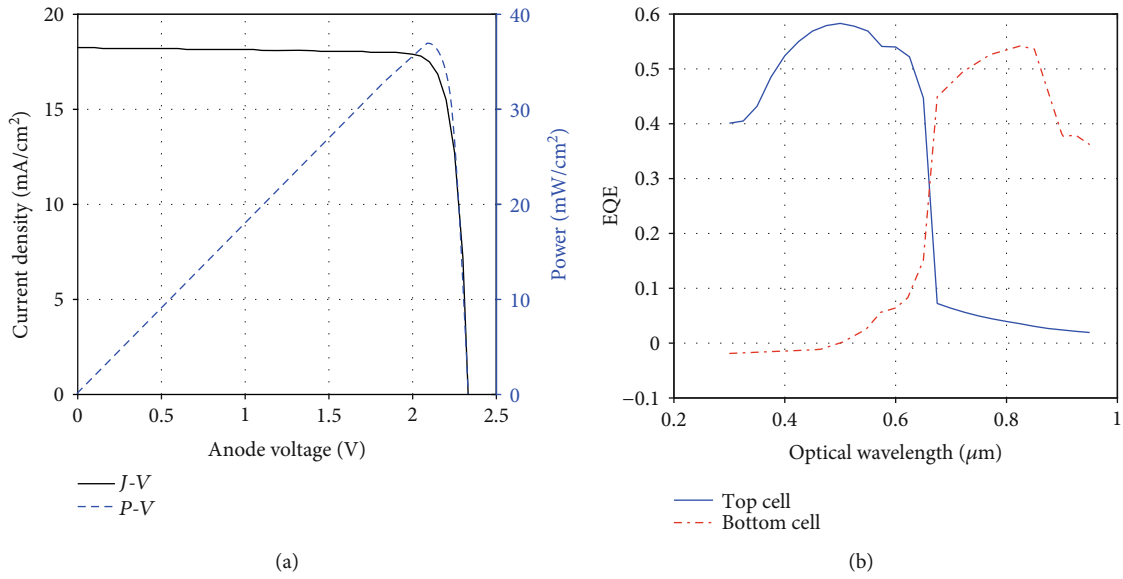

Figure 6: Simulation results of the optimized DJ solar cell using $Al_{0.8}Ga_{0.2}As$. (a) J-V characteristic and P-V curve. (b) EQE curve.

cell from its J-V characteristics are $V_{OC} = 2.33$ V, $J_{SC} = 18.23$ mA/cm^2, FF = 86.42%, and a conversion efficiency $\eta_c = 36.71\%$. Moreover, from the P-V curve, the maximum power is 36.74 mW/cm^2. Also, the voltage at which the maximum power occurred is 2.1 V. At this point, the maximum current density is 17.49 mA/cm^2.

In order to measure the optical performance, the external quantum efficiency (EQE) is presented [23]. For the presented DJ InGaP/GaAs cell, the InGaP top cell is responsible for the collection of the first part of the input solar radiation spectrum while the GaAs bottom cell is responsible for the absorption of the long wavelengths based on its energy gap [20]. Figure 6(b) illustrates the simulation of the optimized DJ solar cell EQE under AM1.5G illumination. It is obvious that the InGaP top cell absorbs the photons for the wavelength in the range of 0.3 to 0.65 μm. Regarding the GaAs bottom cell, it absorbs the wavelengths between 0.65 and 0.9 μm.

To give physical insight into the behavior of the cell, Figure 7(a) shows a cutline view of the electrostatic potential whereas Figure 7(b) depicts a detailed photogeneration rate across the device length. The electrostatic potential is maximum at the tunnel junction region. Also, the maximum photogeneration rate occurs at the surface of the device as it is exposed to the maximum solar radiation.

3.2. Using AlGaInP as the Top Window Layer. In this section, the performance optimization of the InGaP/GaAs DJ cell is carried out by using AlGaInP as the top window layer. The same optimization steps of the previous section are carried out except that the optimum Al mole fraction is selected from a recent research work [24, 44], $(Al_{0.7}Ga_{0.3})_{0.5}In_{0.5}P$. The

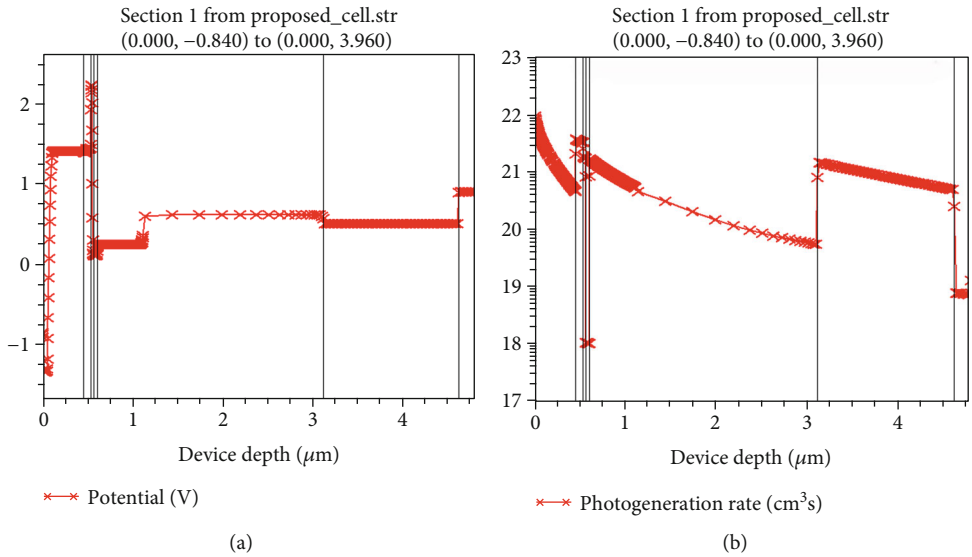

Figure 7: Cutline view of (a) electrostatic potential and (b) logarithmic distribution of the photogeneration rate in the cell.

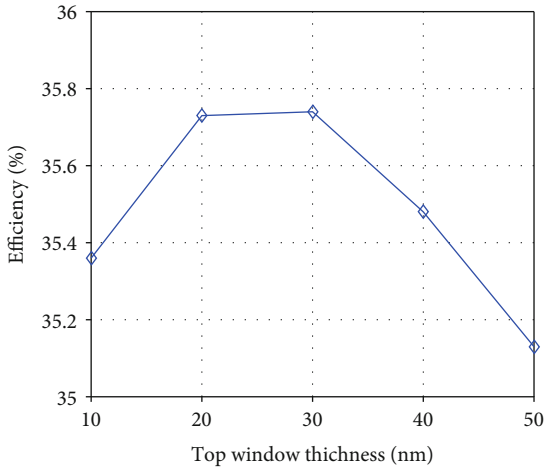

Figure 8: DJ cell efficiency vs. top window layer thickness.

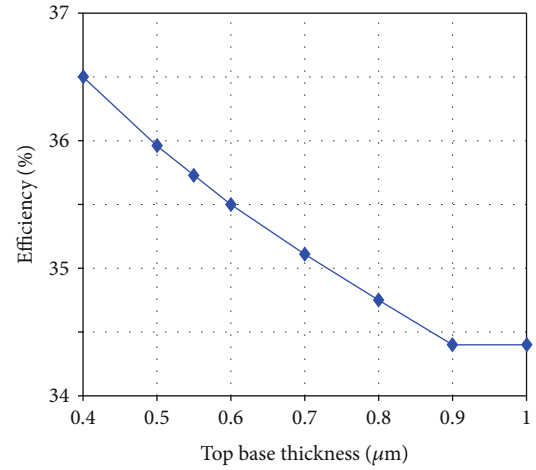

Figure 9: DJ cell efficiency vs. top base thickness.

window layer thickness, top base thickness, bottom BSF layer thickness, and doping are optimized to get the maximum possible efficiency. Then, the *I-V* and *P-V* characteristics are presented along with the EQE and the electrostatic potential and photogeneration rate.

3.2.1. Optimization of Different Layers. Figure 8 shows the impact of the top window layer thickness on efficiency. The maximum efficiency is 35.726% which occurs at an optimized thickness of 0.03 μm. Further, Figure 9 shows the influence of the top base thickness on the efficiency. It is obvious from the figure that the optimum top base thickness is 0.4 μm at which the efficiency is 36.5%.

Regarding the bottom BSF layer, its thickness and doping are to be optimized as in the previous section. Figure 10 shows the influence of the bottom BSF layer thickness (Figure 10(a)) and doping (Figure 10(b)) on the efficiency. As indicated in Figure 10(a), the efficiency increases as the layer thickness varies from 0.2 μm to 1 μm. Beyond the thickness of 1 μm, the efficiency is nearly unchanged. Thus, an optimum thickness of the bottom BSF layer is 1 μm at 38.15% efficiency. As can be deduced from Figure 11(b), the efficiency rises as the doping of the bottom BSF layer increases. So, the optimum doping concentration is 3×10^{19} cm^{-3}, which is the maximum allowable doping concentration of n-type [45, 46], which gives 38.53% efficiency.

3.2.2. Electrical and Optical Performance. Figure 11(a) shows the simulated *J-V* characteristic and *P-V* curve of the optimized DJ cell using $(Al_{0.7}Ga_{0.3})_{0.5}In_{0.5}P$. The extracted electrical performance parameters are $V_{OC} = 2.32$ V, $J_{SC} = 19.84$ mA/cm^2, FF = 83.9%, and $\eta_c = 38.53\%$. From the *P-V* curve, the maximum power obtained is 38.56 mW/cm^2. Also, the voltage at which the maximum power occurred is 2.1 V and the maximum current density is 18.81 mA/cm^2. Finally, Figure 11(b) shows the simulation of the optimized EQE using

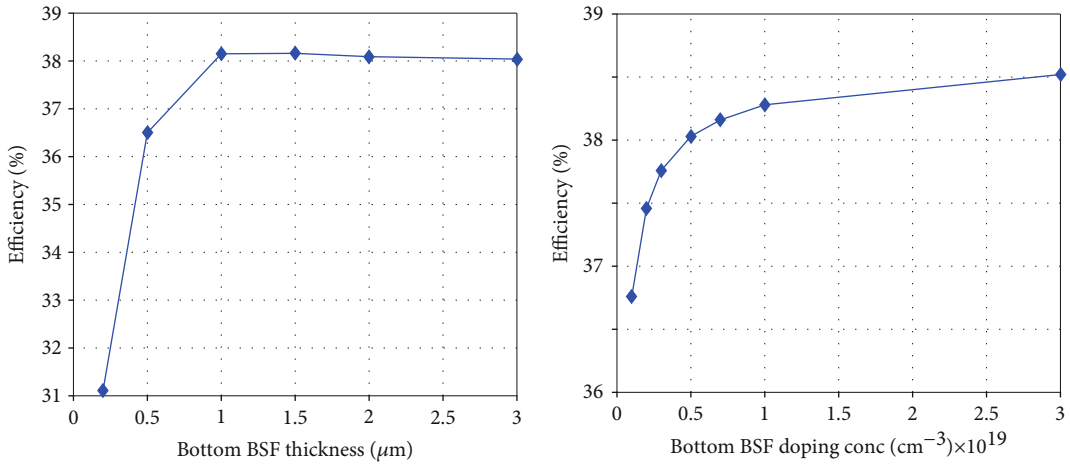

FIGURE 10: Optimization of the bottom BSF parameters. (a) Cell efficiency vs. thickness. (b) Cell efficiency vs. doping concentration.

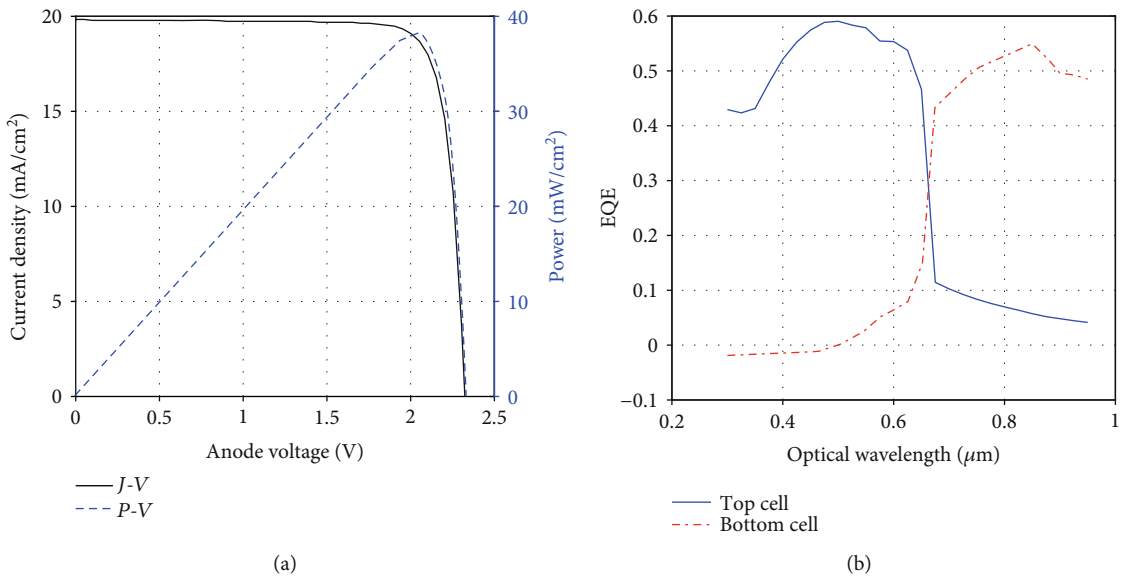

FIGURE 11: Simulation results of the optimized DJ solar cell using $(Al_{0.7}Ga_{0.3})_{0.5}In_{0.5}P$. (a) J-V characteristic and P-V curve. (b) EQE curve.

$(Al_{0.7}Ga_{0.3})_{0.5}In_{0.5}P$ under AM1.5G illumination. The InGaP top cell absorbs the photons for the wavelength in the range of 0.3 to 0.65 μm while the GaAs bottom cell absorbs the wavelengths between 0.65 and 0.9 μm.

For a physical understanding of some phenomena occurring inside the DJ cell, the electrostatic potential and photogeneration rate through the cell length are plotted in Figure 12. Figure 12(a) shows a cutline view of the electrostatic potential in the different layers where the maximum potential is at the tunnel junction region and it decreases when moving away from the tunnel junction. Figure 12(b) shows a cutline view of the photogeneration rate along with the cell depth. Regarding the BSF layers, they reduce the scattering of charge carriers; this means there is an accumulation of charge carriers near the BSF layers. Thus, the photogeneration rate increases at the BSF layers as can be depicted in the figure. So, these layers passivate the surface recombination between the base of the top cell and the emitter of the tunnel diode as well as the tunnel diode contact and the substrate of the bottom cell.

3.3. Comparison between Using $Al_{0.8}Ga_{0.2}As$ and $(Al_{0.7}Ga_{0.3})_{0.5}In_{0.5}P$ as the Top Window Layer. Table 4 shows a summary for the extracted electrical performance parameters for both the optimized InGaP/GaAs DJ cells using the two different top window layers, $Al_{0.8}Ga_{0.2}As$ and $(Al_{0.7}Ga_{0.3})_{0.5}In_{0.5}P$. From the table, it is obvious that the overall performance of the InGaP/GaAs cell is enhanced by using $(Al_{0.7}Ga_{0.3})_{0.5}In_{0.5}P$ over $Al_{0.8}Ga_{0.2}As$ as the cell efficiency increases by 1.82%.

Thus, the $(Al_{0.7}Ga_{0.3})_{0.5}In_{0.5}P$ is found to be superior to $Al_{0.8}Ga_{0.2}As$ as a top window layer material. The reason is that it has a wider and direct bandgap (2.3 eV) rather than

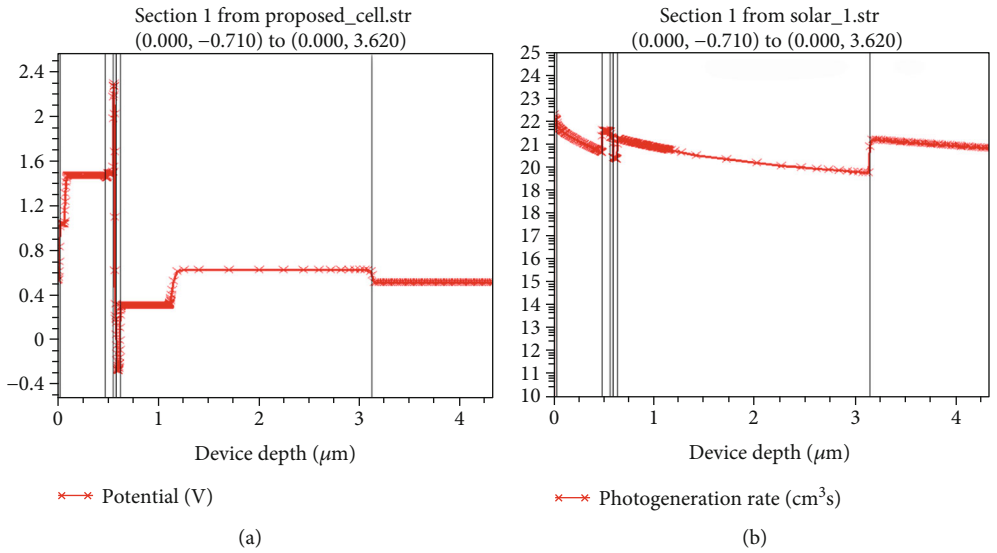

Figure 12: Cutline view of the (a) electrostatic potential and (b) logarithmic distribution of the photogeneration rate in the cell.

Table 4: Summary of the extracted electrical performance parameters for the optimized InGaP/GaAs DJ solar cell using $Al_{0.8}Ga_{0.2}As$ and $(Al_{0.7}Ga_{0.3})_{0.5}In_{0.5}P$.

InGaP/GaAs DJ solar cell	V_{OC} (V)	J_{SC} (mA/cm^2)	FF (%)	η (%)
Top window layer $Al_{0.8}Ga_{0.2}As$	2.33	18.23	86.42	36.71
Top window layer $(Al_{0.7}Ga_{0.3})_{0.5}In_{0.5}P$	2.33	19.84	83.9	38.53

Table 5: Comparison of simulated performance parameters of different DJ solar cells under 1 sun of the standard AM1.5G solar spectrum at 300 K.

	V_{OC} (V)	J_{SC} (mA/cm^2)	FF (%)	η_c (%)
Lueck et al. [19]	2.32	10.9	79.00	23.6
Leem et al. [20]	2.3	10.61	87.55	25.14
Singh and Sarkar [21]	2.39	16.1	87.52	32.196
Nayak et al. [23]	2.66	17.33	88.67	34.52
InGaP/GaAs DJ solar cell with $(Al_{0.7}Ga_{0.3})_{0.5}In_{0.5}P$ as the top window	2.32	19.84	83.9	38.53

the indirect bandgap of $Al_{0.8}Ga_{0.2}As$ (2.09 eV). Thus, $(Al_{0.7}Ga_{0.3})_{0.5}In_{0.5}P$ has the advantage of being more transparent to light. Moreover, it has less surface recombination loss over $Al_{0.8}Ga_{0.2}As$. This result is clear in the EQE curve using the two different top window layers (see Figures 6(b) and 11(b)). It is obvious that the external quantum yield in the short wavelength region of the spectrum is substantially lower for the solar structure with $Al_{0.8}Ga_{0.2}As$ as a top window compared to that having an $(Al_{0.7}Ga_{0.3})_{0.5}In_{0.5}P$ as a top window. In addition, the J_{SC} for the structure with $Al_{0.8}Ga_{0.2}As$ as a top window is more dependent on the surface-state density than $(Al_{0.7}Ga_{0.3})_{0.5}In_{0.5}P$ [47]. This is because the conduction band offset at the $Al_{0.8}Ga_{0.2}As$/InGaP interface causes band bending in the InGaP emitter which stimulates carrier recombination at the interface. This band bending is less pronounced when using $(Al_{0.7}Ga_{0.3})_{0.5}In_{0.5}P$ as a top window layer [47] which leads to less sensitivity to surface-state density. This is the reason that the improvement by using $(Al_{0.7}Ga_{0.3})_{0.5}In_{0.5}P$ as a top window is mainly observed in the short-circuit current density and hence the cell efficiency.

As a conclusion, the $(Al_{0.7}Ga_{0.3})_{0.5}In_{0.5}P$ proved to be a superior choice for the top window layer for the InGaP/GaAs cell exhibiting 38.53% efficiency, more than the $Al_{0.8}Ga_{0.2}As$ efficiency by 1.82%. Thus, the $(Al_{0.7}Ga_{0.3})_{0.5}In_{0.5}P$ is selected to be the optimum top window layer material for the InGaP/-GaAs DJ solar cell.

4. Comparing the Performance of the Optimum InGaP/GaAs DJ Solar Cell Structure with the Recent Research Studies

Table 5 summarizes the electrical performance parameters of the optimized InGaP/GaAs DJ solar cell using $Al_{0.8}Ga_{0.2}As$ and $(Al_{0.7}Ga_{0.3})_{0.5}In_{0.5}P$. As indicated, the efficiency out of

using $(Al_{0.7}Ga_{0.3})_{0.5}In_{0.5}P$ is superior to that of using $Al_{0.8}Ga_{0.2}As$ as it gives 1.82% higher efficiency. The comparison between our simulation results and some corresponding experimental and theoretical work [19, 20, 23, 36] is included. Our optimized InGaP/GaAs DJ solar cell, with the optimum $(Al_{0.7}Ga_{0.3})_{0.5}In_{0.5}P$ as the top window layer, gives 4% higher conversion efficiency under 1 sun of the standard AM1.5G solar spectrum at 300 K in comparison with Ref. [23]. It should be pointed out here that the simulation study in [23] was performed to optimize and design a double-layer top BSF using the same lattice-matched $In_{0.5}(Al_{0.7}Ga_{0.3})_{0.5}P$ layer. The optimization was carried out by varying the thickness only. In our current study, we have tried not only to optimize the window layer main parameters but also to provide the optimization of other important parameters to obtain the maximum possible efficiency out of this design.

5. Conclusion

In this work, the InGaP/GaAs DJ solar cell is designed, simulated, and optimized. As the window layer is a crucial structural element in designing the DJ cell, it is important to select the most appropriate material and its parameters that give the highest efficiency. So, the device structure is optimized by using AlGaAs and AlGaInP in the window layer of the top cell. The efficiency has been optimized by varying the thickness of the top window layer. Next, the top base thickness, the bottom BSF thickness, and the doping concentration of the bottom BSF are optimized. The simulation results such as *I-V* characteristics, *P-V* characteristics, and EQE are extracted and plotted. A comprehensive simulation study is performed to compare the two materials (AlGaAs and AlGaInP) to determine the best top window layer material. The optimized top window material is found to be $(Al_{0.7}Ga_{0.3})_{0.5}In_{0.5}P$ which is lattice-matched with InGaP and GaAs. For the optimized DJ cell structure, $V_{OC} = 2.32$ V and $J_{SC} = 19.84$ mA/cm^2 are obtained with a significant enhancement of conversion efficiency up to 38.53% under the illumination of 1 sun of the AM1.5G spectrum. This efficiency is about 4% higher in comparison with a similar simulation study. The efficiency improvement, in our current work, is due to the optimization of some parameters along with the window layer main parameters. Finally, the presented work sheds light on the optimization of the InGaP/GaAs DJ solar cell and shows the importance of using accurate numerical TCAD simulations in designing such type of cells that has a lot of different parameters that cannot be optimized experimentally.

Data Availability

No data were used to support this study.

Conflicts of Interest

The authors declare that they have no conflicts of interest.

Acknowledgments

This research has been funded by the Research Deanship of University of Ha'il-Saudi Arabia through project number RG-20047.

References

[1] K. Ranabhat, L. Patrikeev, A. Antal'evna-Revina, K. Andrianov, V. Lapshinsky, and E. Sofronova, "An introduction to solar cell technology," *Journal of Applied Engineering Science*, vol. 14, no. 4, pp. 481–491, 2016.

[2] K.-D. Jäger, O. Isabella, A. H. Smets, R. A. van Swaaij, and M. Zeman, *Solar Energy: Fundamentals, Technology and Systems*, UIT Cambridge, 2016.

[3] W. Wei, H. Wang, C. Wang, and H. Luo, "Advanced nanomaterials and nanotechnologies for solar energy," *International Journal of Photoenergy*, vol. 2019, 2 pages, 2019.

[4] D. H. Phuc and H. T. Tung, "Band tunable CdSe quantum dot-doped metals for quantum dot-sensitized solar cell application," *International Journal of Photoenergy*, vol. 2019, 8 pages, 2019.

[5] M. Salem, A. Zekry, A. Shaker, and M. Abouelatta, "Design and simulation of proposed low cost solar cell structures based on heavily doped silicon wafers," in *2016 IEEE 43rd Photovoltaic Specialists Conference (PVSC)*, pp. 2393–2397, Portland, OR, USA, 2016.

[6] M. S. Salem, A. Zekry, A. Shaker, M. Abouelatta, and T. M. Abdolkader, "Performance enhancement of a proposed solar cell microstructure based on heavily doped silicon wafers," *Semiconductor Science and Technology*, vol. 34, no. 3, article 035012, 2019.

[7] A. Luque and S. Hegedus, *Handbook of Photovoltaic Science and Engineering*, John Wiley & Sons, 2011.

[8] S. Kozhukhovskaia, E. Filimonov, and M. Shvarts, "Experimental model of multi-junction solar cell: IV curve tailoring and photoresponce artifact simulation," *Journal of Physics: Conference Series*, vol. 586, no. 1, article 012014, 2015.

[9] N. Pakhanov, V. Andreev, M. Shvarts, and O. Pchelyakov, "State-of-the-art architectures and technologies of high-efficiency solar cells based on III–V heterostructures for space and terrestrial applications," *Optoelectronics, Instrumentation and Data Processing*, vol. 54, no. 2, pp. 187–202, 2018.

[10] T. Thomas, A. Mellor, N. P. Hylton et al., "Requirements for a GaAsBi 1 eV sub-cell in a GaAs-based multi-junction solar cell,," *Semiconductor Science and Technology*, vol. 30, no. 9, article 094010, 2015.

[11] K. Tanabe, "A review of ultrahigh efficiency III-V semiconductor compound solar cells: multijunction tandem, lower dimensional, photonic up/down conversion and plasmonic nanometallic structures," *Energies*, vol. 2, no. 3, pp. 504–530, 2009.

[12] Y. Guo, Q. Liang, B. Shu, J. Wang, and Q. Yang, "The III–V triple-junction solar cell characteristics and optimization with a Fresnel lens concentrator," *International Journal of Photoenergy*, vol. 2018, 10 pages, 2018.

[13] K. Attari, L. Amhaimar, A. Asselman, and M. Bassou, "The design and optimization of GaAs single solar cells using the genetic algorithm and Silvaco ATLAS," *International Journal of Photoenergy.*, vol. 2017, pp. 1–7, 2017.

[14] B. Kınacı, Y. Özen, T. Asar et al., "Study on growth and characterizations of $Ga_xIn_{1-x}P$/GaAs solar cell structure," *Journal of Materials Science: Materials in Electronics*, vol. 24, pp. 3269–3274, 2013.

[15] Y. Özen, N. Akın, B. Kınacı, and S. Özçelik, "Performance evaluation of a GaInP/GaAs solar cell structure with the integration of AlGaAs tunnel junction," *Solar Energy Materials and Solar Cells, Volume*, vol. 137, pp. 1–5, 2015.

[16] R. Ferrini, G. Guizzetti, M. Patrini, A. Parisini, L. Tarricone, and B. Valenti, "Optical functions of InGaP/GaAs epitaxial layers from 0.01 to 5.5 eV," *European Physical Journal B - Condensed Matter*, vol. 27, pp. 449–458, 2002.

[17] S. Mangal, P. Ghelfi, A. Bogoni, and P. Banerji, "Barrier height dependence of Fano factor and 1/fnoise effect on InGaP based Schottky barrier diode," *Journal of Applied Physics*, vol. 110, no. 3, p. 033721, 2011.

[18] R. Oshima, Y. Nagato, Y. Okano, and T. Sugaya, "Enhancement of open-circuit voltage in InGaP solar cells grown by solid source molecular beam epitaxy," *Japanese Journal of Applied Physics*, vol. 57, no. 8S3, article 08RD07, 2018.

[19] M. Lueck, C. Andre, A. Pitera, M. Lee, E. Fitzgerald, and S. Ringel, "Dual junction GaInP/GaAs solar cells grown on metamorphic SiGe/Si substrates with high open circuit voltage," *IEEE Electron Device Letters*, vol. 27, no. 3, pp. 142–144, 2006.

[20] J. Leem, Y. Lee, and J. Yu, "Optimum design of InGaP/GaAs dual-junction solar cells with different tunnel diodes," *Optical and Quantum Electronics*, vol. 41, no. 8, pp. 605–612, 2009.

[21] K. J. Singh and S. K. Sarkar, "An effective modeling approach for high efficient solar cell using virtual wafer fabrication tools," *Journal of Nano-and Electronic Physics*, vol. 3, no. 1, p. 792, 2011.

[22] K. J. Singh and S. K. Sarkar, "Highly efficient ARC less InGaP/-GaAs DJ solar cell numerical modeling using optimized InAlGaP BSF layers," *Optical and Quantum Electronics*, vol. 43, no. 1-5, pp. 1–21, 2012.

[23] P. Nayak, J. Dutta, and G. Mishra, "Efficient InGaP/GaAs DJ solar cell with double back surface field layer," *Engineering Science and Technology, an International Journal*, vol. 18, no. 3, pp. 325–335, 2015.

[24] 1J. Dutta, P. Nayak, and G. Mishra, "Design and evaluation of ARC less InGaP/GaAs DJ solar cell with InGaP tunnel junction and optimized double top BSF layer," *Optik*, vol. 127, no. 8, pp. 4156–4161, 2016.

[25] K. W. A. Chee and Y. Hu, "Design and optimization of ARC less InGaP/GaAs single-/multi-junction solar cells with tunnel junction and back surface field layers," *Superlattices and Microstructures*, vol. 119, pp. 25–39, 2018.

[26] F. Djaafar, B. Hadri, and G. Bachir, "Optimal parameters for performant heterojunction InGaP/GaAs solar cell," *International Journal of Hydrogen Energy*, vol. 42, no. 13, pp. 8644–8649, 2017.

[27] S. Hungyo, K. J. Singh, and R. S. Dhar, "Cell thickness optimization of dual junction InGaP/GaAs solar cell against temperature variation," in *2019 Devices for Integrated Circuit (DevIC)*, pp. 281–285, Kalyani, India, 2019.

[28] T. Aihara, T. Tayagaki, R. Oshima et al., "Analysis of subcell open-circuit voltages of InGaP/GaAs dual-junction solar cells fabricated using hydride vapor phase epitaxy," *Japanese Journal of Applied Physics*, vol. 59, no. SG, p. SGGF02, 2020.

[29] L. Wang, J. He, X. Shang et al., "Enhanced tunneling in the GaAs p+–n+ junction by embedding InAs quantum dots," *Semiconductor Science and Technology*, vol. 27, no. 11, article 115010, 2012.

[30] *ATLAS User's Manual: A 2D Numerical Device Simulator*, Silvaco, 2016.

[31] J. Plá, M. Barrera, and F. Rubinelli, "The influence of the InGaP window layer on the optical and electrical performance of GaAs solar cells," *Semiconductor Science and Technology*, vol. 22, no. 10, pp. 1122–1130, 2007.

[32] H. W. Yu, C. C. Chung, C. te Wang et al., "InGaP/GaAs dual-junction solar cell with AlGaAs/GaAs tunnel diode grown on 10 off misoriented GaAs substrate," *Japanese Journal of Applied Physics*, vol. 51, no. 8R, article 080208, 2012.

[33] M. H. Tsutagawa and S. Michael, "Triple junction InGaP/-GaAS/Ge solar cell optimization: the design parameters for a 36.2% efficient space cell using Silvaco ATLAS modeling & simulation," in *2009 34th IEEE Photovoltaic Specialists Conference (PVSC)*, pp. 001954–001957, Philadelphia, PA, USA, 2009.

[34] G. Sahoo, P. Nayak, and G. Mishra, "An ARC less InGaP/GaAs DJ solar cell with hetero tunnel junction," *Superlattices and Microstructures*, vol. 95, pp. 115–127, 2016.

[35] H. Arzbin and A. Ghadimi, "Efficiency improvement of ARC less InGaP/GaAs DJ solar cell with InGaP tunnel junction and optimized two BSF layer in top and bottom cells," *Optik*, vol. 148, pp. 358–367, 2017.

[36] K. J. Singh and S. K. Sarkar, "A wide band gap In 0.5 (Al 0.7 Ga 0.3) 0.5 P back surface field layer increases 6% more efficiency in DLAR dual junction InGaP solar cell," in *2016 International Conference on Energy Efficient Technologies for Sustainability (ICEETS)*, pp. 182–186, Nagercoil, India, 2016.

[37] A. Kirk, "High efficacy thinned four-junction solar cell," *Semiconductor science and technology*, vol. 26, no. 12, article 125013, 2011.

[38] M. Yamaguchi, K.-H. Lee, K. Araki, N. Kojima, and Y. Ohshita, "(Invited) Potential and activities of III-V/Si tandem solar cells," *ECS Transactions*, vol. 69, no. 4, pp. 11–20, 2015.

[39] Y. Zhao, J. S. Xue, J. C. Zhang, X. W. Zhou, Y. C. Zhang, and Y. Hao, "InAlN/InGaN/GaN double heterostructure with improved carrier confinement and high-temperature transport performance grown by metal-organic chemical vapor deposition," *Semiconductor Science and Technology*, vol. 30, no. 7, article 075005, 2015.

[40] T. Kehagias, N. Florini, J. Kioseoglou et al., "Nanostructure and strain properties of core-shell GaAs/AlGaAs nanowires," *Semiconductor Science and Technology*, vol. 30, no. 11, article 114012, 2015.

[41] C. Grasse, G. Boehm, M. Mueller, T. Gruendl, R. Meyer, and M. Amann, "Empirical modeling of the refractive index for (AlGaIn) As lattice matched to InP," *Semiconductor science and technology*, vol. 25, no. 4, article 045018, 2010.

[42] S. M. Sze and K. K. Ng, *Physics of Semiconductor Devices*, John wiley & sons, 2006.

[43] S. Abbasian and R. Sabbaghi-Nadooshan, "Design and evaluation of ARC less InGaP/AlGaInP DJ solar cell," *Optik*, vol. 136, pp. 487–496, 2017.

[44] B. Galiana, I. Rey-Stolle, M. Baudrit, I. García, and C. Algora, "A comparative study of BSF layers for GaAs-based single-junction or multijunction concentrator solar cells,"

Semiconductor science and technology, vol. 21, no. 10, pp. 1387–1392, 2006.

[45] E. F. Schubert, *Doping in III-V Semiconductors*, E. Fred Schubert, 2015.

[46] S. Siebentritt and U. Rau, *Wide-Gap Chalcopyrites*, Springer, 2006.

[47] A. S. Gudovskikh, N. A. Kalyuzhnyy, V. M. Lantratov, S. A. Mintairov, M. Z. Shvarts, and V. M. Andreev, "Properties of interfaces in GaInP solar cells," *Semiconductors*, vol. 43, no. 10, pp. 1363–1368, 2009.